

LONG-TERM SHORELINE EVOLUTION MODELING IN EMBAYED BEACHES

Yen Tran Hai¹ and Eric Barthélemy¹

Abstract

This paper addresses the feasibility of a combined model that includes longshore sediment transport effects in a cross-shore shoreline evolution model. Longshore transport produces long-term changes of the beach morphology and shoreline position. The longshore contribution is worked out on the basis of the one-line approach in which the shoreline position in time depends on the alongshore gradient of the volumetric sediment transport rate. The analysis provides a relationship between the equilibrium shoreline angle and the wave forcing direction. It also yields a shoreline evolution equation generated by the sole longshore transport. This model is included in the Splinter *et al.* (2014) behavioral model. This combined model was calibrated on the Narrabeen semi-embayed beach data (Turner *et al.*, 2016). The results are that the combined model is able to reproduce the shoreline trends and that the longshore component contributes to the seasonal shoreline fluctuations.

Key words: shoreline evolution model, longshore model, embayed beach, one-line model

1. Introduction

Long-term modeling (decades) of shoreline changes cannot be easily challenged with physics based models. The best alternative is to use simple behavioral template models (Davidson & Turner, 2009), all the complex cross-shore erosion/accretion processes being encapsulated in a few parameters. Most of these cross-shore models draw on the phenomenological idea that a beach relaxes towards equilibrium (Wright & Short, 1984; Kriebel & Dean, 1993). Calibrated against reliable data series of cross-shore changes, this type of model reaches good predictive skills (Splinter *et al.*, 2014; Castelle *et al.*, 2014). A constant is usually added to the model equation to account for unexplained shoreline motions such as long-term trends uncorrelated with wave climate changes at small time scales (days or weeks). However, the long-term shoreline variations are the result of complicated processes and just one constant free parameter is not sufficient. The shoreline model needs thus to be improved by taking into account the longshore process expressed by a better parameterization.

Amongst the processes not accounted for are the longshore transport gradients contributions to the shoreline changes. These gradients of course are important in non-straight shorelines such as embayed beaches (Turki *et al.*, 2013). The curvature of an embayed beach shoreline is related to the refraction and diffraction of the waves as they propagate from deep waters towards the breaking point. A stretch of beach is at equilibrium if the time average wave direction is orthogonal to the shoreline. Any wave forcing which departs from that average direction will create a longshore sediment transport and since the shoreline orientation changes alongshore, it produces a transport gradient that results in changes of shoreline position. To account for this, a one-line approach is adopted.

In section 2.1, the cross-shore model of Splinter *et al.* (2014) (hereinafter called STDBCO14) is recalled and was implemented for sake of comparison. The longshore model which is suggested by supplementing the shoreline model is presented in section 2.2. The combined model is presented in section 2.3. The shoreline evolution models were calibrated on Narrabeen beach data (Turner *et al.*, 2015) which is now open access and described in section 3. The model result analysis is mentioned in section 4. Section 5 is for the discussion and conclusion.

¹ LEGI, University of Grenoble (UGA), BP53, 38041 Grenoble cedex9, France. hai-yen.tran@univ-grenoble-alpes.fr

¹ LEGI, University of Grenoble (UGA), BP53, 38041 Grenoble cedex9, France. eric.barthelemy@grenoble-inp.fr

2. Methods

2.1. Cross-shore model

The STDBCO14 cross-shore shoreline model reads:

$$\frac{dS}{dt} = c(F^+ + rF^-) + d \quad (1)$$

where $S(t)$ is the shoreline position in the transect, t is time in days, c ($\text{m}^{1.5}\text{days}^{-1}\text{W}^{-0.5}$) and d (m/days) are free parameters adjusted by an optimization method. The forcing term F is defined by (Splinter *et al.*, 2014):

$$F = P^{0.5} \frac{\Delta\Omega}{\sigma_{\Delta\Omega}} \quad (2)$$

where P is the incident wave power; $\Omega(t)$ is the dimensionless fall velocity of Gourlay number:

$$\Omega = \frac{H_s \omega_s}{T_p}; H_s \text{ is the significant wave height; } T_p \text{ is the peak wave period; } \omega_s \text{ is the sediment fall velocity}$$

(Cheng, 1997). $\Delta\Omega$ is the disequilibrium dimensionless fall velocity, $\Delta\Omega = \Omega_0(t) - \Omega(t)$; $\sigma_{\Delta\Omega}$ is the standard deviation of $\Delta\Omega$. The equilibrium dimensionless fall velocity $\Omega_0(t)$ is defined by (Wright and Short, 1984; Davidson *et al.*, 2013):

$$\Omega_0(t) = \frac{\sum_{j=0}^{D/\Delta t} \Omega_j 10^{-j\Delta t/\phi}}{\sum_{j=0}^{D/\Delta t} 10^{-j\Delta t/\phi}} \quad (3)$$

where ϕ (days) is the 'memory decay', $D = 2\phi$, Δt is the forcing survey time interval, j is the number of data points in the survey time series prior to the calculation point at time t (Davidson *et al.*, 2013).

The forcing term F is differentiated between accretion and erosion with F^+ and F^- , respectively. If $F > 0$, $F = F^+$. Conversely, if $F < 0$, $F = F^-$. The parameter r called the erosion ratio is the ratio of accretionary component to erosional component (Splinter *et al.*, 2014):

$$r = \left| \frac{\sum_{i=0}^N F_i^+}{\sum_{i=0}^N F_i^-} \right| \quad (4)$$

where N is the total record length (Splinter *et al.*, 2014), F_i^+ and F_i^- are the measured forcing functions.

2.2. Longshore model

In equation (1), d represents the long-term trend of the shoreline evolution and all unexplained shoreline motions. Amongst the main unexplained shoreline motions are of course those related to the longshore sediment drift. In equation (1), the constant d is replaced by a model accounting for this longshore drift of sediment. Wave incidence will trigger a longshore drift and since the drift magnitude depends on the shoreline orientation a gradient in longshore transport is possible that it will produce a shoreline position change. This is particularly true in embayed beaches exhibiting curvatures.

Our underlying assumption is thus that for oblique waves the cross-shore component of the wave energy feeds into specific shoreline motions described by (1) and that alongshore wave energy transferred to the transport drift generates shoreline variability for beaches with alongshore orientation variability. The volumetric longshore sediment transport rate Q is written (Reeve, 2004; Idier *et al.*, 2011):

$$Q = K_1 H_{s,b}^{5/2} \sin 2(\alpha_b(t) - \beta(x)) = K_1 H_{s,b}^{5/2} \sin 2\theta \quad (5)$$

$$\theta = \alpha_b(t) - \beta(x) \quad (6)$$

where K_1 is a constant defined by sediment characteristics, $K_1 \approx 0.1$ to $0.2 \text{ m}^{1/2}\text{s}^{-1}$; $H_{s,b}$ is the significant wave height at breaking point; $\beta(x)$ is the shoreline orientation, $\alpha_b(t)$ is the orientation of incident wave field (Fig. 1).

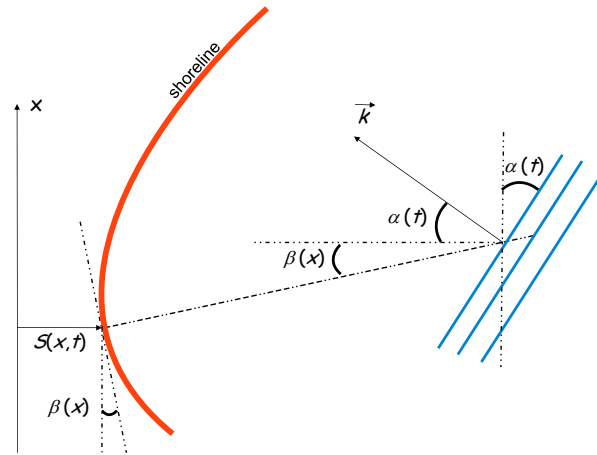


Figure 1: Definition of wave angle and shoreline angle. From the horizontal line, an angle measured clockwise is positive and an angle measured counterclockwise is negative.

The relationship between the shoreline position and the volumetric longshore transport rate is (Pelnard-Considère, 1956):

$$\frac{\partial S}{\partial t} = -\frac{1}{h_c} \frac{\partial Q}{\partial x} \quad (7)$$

where h_c is the closure depth.

2.2.1. Equilibrium shoreline orientation

The most important issue of shoreline evolution modeling is how to define the equilibrium state of the shoreline since it is always an evolving quantity. We assume that any quantity can be decomposed into a mean and fluctuating contribution. The mean of a given random function $f(t)$ over a given time scale T_c is classically defined by:

$$\overline{f(t)} = \frac{1}{T_c} \int_{t_0}^{t_0+T_c} f(t) dt$$

(8)

Applying operator (8) to equation (7) yields:

$$\frac{\partial \overline{S}}{\partial t} = -\frac{1}{h_c} \frac{\partial \overline{Q}}{\partial x} \quad (9)$$

Equation (9) is used to determine the equilibrium state of the shoreline orientation. The shoreline reaches the equilibrium orientation when the volumetric longshore transport rate does not change along the shoreline. In order to obtain from (5) \bar{Q} , the wave angle α_b and shoreline angle β are in turn split into means and fluctuations:

$$\alpha_b = \bar{\alpha}_b + \alpha'_b; \quad \beta = \bar{\beta} + \beta' \quad (10)$$

Consequently,

$$\bar{\theta} = \bar{\alpha}_b - \bar{\beta}; \quad \theta' = \alpha'_b - \beta' \quad (11)$$

$$\bar{Q} = K_1 \sin 2\bar{\theta} \overline{H^{5/2} \cos 2\theta'} + K_1 \cos 2\bar{\theta} \overline{H^{5/2} \sin 2\theta'} \quad (12)$$

The equilibrium shoreline position $\bar{S}(x)$ is such that:

$$\frac{\partial \bar{S}}{\partial t} = 0 \quad (13)$$

which implies:

$$\frac{\partial \bar{Q}}{\partial x} = 0 \Rightarrow \bar{Q} = cte \quad (14)$$

For embayed beach which is a closed system with no sediment exchange with the rest of the coastal zone, we have:

$$\bar{Q} = 0 \Rightarrow \sin 2\bar{\theta} \overline{H^{5/2} \cos 2\theta'} + \cos 2\bar{\theta} \overline{H^{5/2} \sin 2\theta'} = 0 \quad (15)$$

It is noted that if the wave height is completely uncorrelated with the wave direction, $\overline{H^{5/2} \cos 2\theta'}$ and $\overline{H^{5/2} \sin 2\theta'}$ are zero and thus any value of $\bar{\theta}$ is possible in (15). On the contrary, if wave height correlates with the propagation direction, the average longshore sediment flux (12) can be written as:

$$\bar{Q} = K_1 \sin(2\bar{\theta} + \varphi) \quad \text{with} \quad \tan \varphi = \frac{\overline{H^{5/2} \sin 2\theta'}}{\overline{H^{5/2} \cos 2\theta'}} \quad (16)$$

The coastline does not change as fast as the forcing condition, it is therefore reasonable to believe that the fluctuations of the shoreline angle β' are small compared to α'_b , so from (11):

$$\theta' = \alpha'_b \quad (17)$$

$$\tan \varphi \simeq \frac{\overline{H^{5/2} \sin 2\alpha'_b}}{\overline{H^{5/2} \cos 2\alpha'_b}} \quad (18)$$

Solving equation (15) for $\bar{\beta}$ gives:

$$\bar{\beta}(x) = \bar{\alpha}_b(x) + \frac{1}{2} \varphi(x) \quad (19)$$

The equilibrium shoreline orientation and the average breaking wave propagation direction need to meet the condition (19). The value of φ is defined by equation (18) using the wave height and the breaking wave angle fluctuation. If the value of $\frac{1}{2}\varphi(x)$ is small (see section 3), $\bar{\beta}(x)$ is approximately $\bar{\alpha}_b(x)$, the average wave direction is thus perpendicular to the shoreline.

2.2.2. Longshore component

The shoreline evolution derived from longshore drift is expressed by combining equation (5) and equation (7):

$$\frac{\partial S}{\partial t} = -\frac{K_1}{h_c} \frac{d}{dx} \left(H_{s,b}^{5/2} \sin 2\theta \right) = -\frac{K_1}{h_c} H_{s,b}^{3/2} \left[2H_{s,b} \cos 2\theta \frac{d\theta}{dx} + \frac{5}{2} \sin 2\theta \frac{dH_{s,b}}{dx} \right] \quad (20)$$

$$\theta = \alpha_b(x, t) - \beta(x) = \bar{\alpha}_b(x) - \beta(x) + \alpha'_b(x, t) = \alpha'_b(x, t) + \varepsilon \quad (21)$$

$$A = -2 \frac{K_1}{h_c} \left[2H_{s,b} \frac{d\theta}{dx} \cos 2\varepsilon + \frac{5}{2} \frac{dH_{s,b}}{dx} \sin 2\varepsilon \right] \quad (22)$$

$$B = -2 \frac{K_1}{h_c} \left[-2H_{s,b} \frac{d\theta}{dx} \sin 2\varepsilon + \frac{5}{2} \frac{dH_{s,b}}{dx} \cos 2\varepsilon \right] \quad (23)$$

In which, it is assumed that $\bar{\alpha}_b(x) \approx \beta(x)$ with an error of $\varepsilon(x)$. The functions A and B are non-dimensional. The parameters A and B contain derivatives with respect to x . It will be assumed that the derivatives of wave parameters with respect to x are constant in time on a given transect. Therefore, a model is suggested from equation (20) which reads:

$$\frac{dS}{dt} = H_{s,b}^{3/2} [a \cos 2\alpha'_b + b \sin 2\alpha'_b] \quad (24)$$

with a and b non-dimensional parameters to be fitted.

2.3. Combined model

The combined model consists in adding the longshore model (24) to the cross-shore model (1) in place of the free parameter d of equation (1). The model can be written as:

$$\frac{dS}{dt} = c(F^+ + rF^-) + H_{s,b}^{3/2} [a \cos 2\alpha'_b + b \sin 2\alpha'_b] \quad (25)$$

The free parameters a , b and c ($m^{1.5}d^{-1}W^{-0.5}$) play a significant role in the model in regulating the magnitude of shoreline change rate. In order to find the free parameter values in the model, a global optimization method by the Simulated Annealing was used to minimize the root-mean-square error (RMSE) of shoreline changes between measurements and model (Castelle *et al.*, 2014). The R package *GenSA* was used to solve the optimization problem. Model skill indicators are defined in much the same way as Splinter *et al.* (2014). The RMSE is defined by:

$$RMSE = \sqrt{\frac{\sum_{i=0}^N (S_i - S_{m_i})^2}{N}} \quad (26)$$

where S_i is the i th measured shoreline position and S_{m_i} is the modeled shoreline position at the same date. The 1st modeled shoreline position is taken equal to the 1st measured shoreline position ($S_{m_1} = S_1$).

The results can also be evaluated with the NMSE (normalized mean square error), which is defined as Splinter *et al.* (2014):

$$\text{NMSE} = \frac{\sum_{i=0}^N (S_i - S_{m_i})^2}{\sum_{i=0}^N (S_i - \bar{S})^2} \quad (27)$$

where \bar{S} is the mean value of measured shoreline data. If $\text{NMSE} = 0$, the model perfectly captures all data points; conversely, if $\text{NMSE} = 1$, the model has no skill.

3. Site and data

Narrabeen is located on Sydney's Northern Beaches in southeast Australia. The wave data which includes the significant wave height H_s , the peak wave period T_p and the wave direction α was collected from January 1979 to October 2014, every 1 h. The monthly shoreline data was collected from April 1976 to February 2016. The 8 year time series data from January 2005 to December 2012 which is identical with calibration time period of Splinter *et al.* (2014) was extracted to calibrate our own models. The shoreline proxy of elevation $z = 0.7$ m corresponding to mean high tide water level was used to calibrate the model. There are five survey-transects which are identified as PF1, PF2, PF4, PF6 and PF8 (Fig. 2). The wave forcing dataset is at 10 m water-depth ($h = 10$ m) location. The mean grain size is of $\phi = 2$ ($d_{50} = 0.4$ mm) along the entire beach (Splinter *et al.*, 2014).

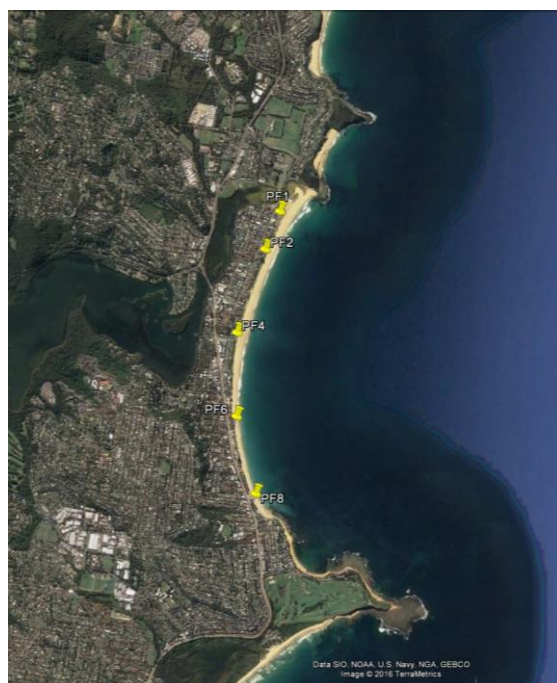


Figure 2. Aerial image of Narrabeen beach. Each transect end is pin-pointed.

The average values of the significant wave height H_s and the dimensionless fall velocity Ω at $h = 10$ m for each transect are shown in Tab. 1. It indicates that H_s at PF1 is stronger than the others, H_s at PF8 is comparatively smaller. The mean value of T_p is of 9.67 s.

The wave climate data at breaking point is refracted from wave data at $h = 10$ m with a breaking significant wave height calculated following Komar (1974):

$$H_{s,b} = 0.39g^{1/5} (T_p H_{10})^{2/5} \quad (28)$$

and the breaking wave angle α_b is calculated using Snell's law as if the bathymetry was 1D.

The average wave angle at $h = 10$ m, $\overline{\alpha}_{10}$, is also shown in Tab. 1. The average value of the wave orientation decreases counterclockwise from the North to the South of the beach, in line with the shoreline orientation.

Table 1. Average value and standard deviation of H_{s10} , $H_{s,b}$, Ω_{10} and α_{10} .

Transect	\overline{H}_{s10} (m)	$\sigma_{H_{s10}}$ (m)	$\overline{H}_{s,b}$ (m)	$\sigma_{H_{s,b}}$ (m)	$\overline{\Omega}_{10}$	$\sigma_{\Omega_{10}}$	$\overline{\alpha}_{10}$ (°)	$\sigma_{\alpha_{10}}$ (°)
PF1	1.15	0.50	1.58	0.33	2.56	1.05	25.61	15.57
PF2	0.98	0.42	1.48	0.31	2.19	0.91	21.49	10.89
PF4	1.06	0.48	1.52	0.33	2.35	1.00	11.70	12.33
PF6	0.94	0.45	1.45	0.32	2.10	0.99	5.04	11.47
PF8	0.77	0.37	1.33	0.28	1.76	0.91	-3.01	10.39

4. Results

4.1. Cross-shore model

Before working on the combined model, we re-implemented the STDBCO14 cross-shore model using Narrabeen beach data. The STDBCO14 cross-shore model was calibrated with both the wave forcing data at $h = 10$ m and at breaking point while Splinter *et al.* (2014) used wave climates at breaking point obtained from numerically refracting waves from 15 m water-depth location to the breaking point. The average value and the standard deviation of H_{s10} and $H_{s,b}$ for each transect are presented in Tab. 1. It shows that the average value of $H_{s,b}$ is larger than that of H_{s10} but the standard deviation of $H_{s,b}$ is smaller than that of H_{s10} . It means that the data variability of $H_{s,b}$ is weaker than that of H_{s10} . This is due to the predictor (28) in which the power 2/5 causes the H_{s10} variability to be diminished.

As a consequence, the standard deviation of the modeled shoreline position with wave forcing at breaking point $\sigma_{S_{H_{s,b}}}$ is smaller than that with wave forcing at $h = 10$ m (Tab. 2). The variability of $S_{H_{s,b}}$ is thus weaker than $S_{H_{s10}}$. The cross-shore model results with wave forcing at $h = 10$ m match more closely those of Splinter *et al.* (2014) than with breaking wave forcing. The suggested combined model described below was thus calibrated with the wave forcing for cross-shore terms at $h = 10$ m and wave forcing for longshore terms at the breaking point using (28).

Table 2. Standard deviation of detrended values of S_{data} , $S_{H_{s,b}}$ and $S_{H_{s10}}$.

Transect	$\sigma_{S_{data}}$ (m)	$\sigma_{S_{H_{s,b}}}$ (m)	$\sigma_{S_{H_{s10}}}$ (m)
PF1	9.95	1.39	3.00
PF2	7.72	3.54	4.47
PF4	9.60	3.13	5.35
PF6	8.36	3.47	4.90
PF8	7.23	4.96	6.35

4.2. Combined model

The values of $\tan \varphi$ and φ in Tab. 3 are calculated with equation (18). It is noticeable that φ is quite small. Accordingly, the average shoreline angle approximates the average breaking wave angle as stated by the equilibrium condition (19). Tab. 3 also shows the measured values of $\overline{\alpha}_b$ and $\overline{\alpha}_{10}$, the computed values of $\overline{\beta}_b$ and $\overline{\beta}_{10}$ with (19) and the measured shoreline angle β_m . The shoreline angle β_m for each transect was measured by using Google Earth images and it is consistent with data of Turner *et al.* (2016). It is

realized that $\overline{\beta_{10}}$ is a closer guess to β_m than $\overline{\beta_b}$ and therefore that with the available data β_m and $\overline{\alpha_{10}}$ are related in a more satisfactory way by equation (19). The value of $\overline{\alpha_{10}}$ will thus be used to calculate the wave angle fluctuation in equation (25).

Fig. 3 shows results of calibrated parameters from the combined model in comparison with those of Splinter *et al.* (2014). The values of ϕ are chosen to get the smallest RMSE and r is calculated following equation (4). Fig. 3 indicates that the differences between our calibrated parameters at several transects and those of Splinter *et al.* (2014) stem from the differences in the input time series data.

Fig. 4, Fig. 5, Fig. 6, Fig. 7 and Fig. 8 show the STDBCO14 cross-shore model (1) outputs and the combined model (25) outputs. The NMSE and smallest RMSE of each transect was presented in Tab. 4. The longshore and cross-shore contributions to the combined model are separately analyzed and shown in Fig. 4, Fig. 5, Fig. 6, Fig. 7 and Fig. 8. Tab. 5 shows results of free parameters a and b of longshore component in the combined model.

Table 3. Values of ϕ , α_b , α_{10} , β_b , β_{10} and β_m (see Fig. 1 for more about angle measurement).

Transect	$\tan \phi$ (18)	ϕ (°)	α_b (°)	α_{10} (°)	β_b (°) (19)	β_{10} (°) (19)	β_m (°)
PF1	0.045	2.60	11.28	25.61	12.58	26.91	27
PF2	0.026	1.48	9.40	21.49	10.14	22.23	20
PF4	0.003	0.17	4.98	11.70	5.07	11.79	14
PF6	-0.011	-0.63	1.79	5.04	1.48	4.73	-5
PF8	-0.030	-1.71	-1.77	-3.01	-2.63	-3.87	-31

Table 4. RMSE and NMSE of the STDBCO14 cross-shore model and the combined model.

Transect	Cross-shore model		Combined model		% difference	
	RMSE (m)	NMSE	RMSE (m)	NMSE	RMSE (m)	NMSE
PF1	8.43	0.72	7.52	0.57	11	23
PF2	6.63	0.62	6.41	0.58	3	7
PF4	8.03	0.63	7.84	0.6	2	5
PF6	6.65	0.4	5.14	0.24	26	50
PF8	5.92	0.42	5.55	0.37	6	13

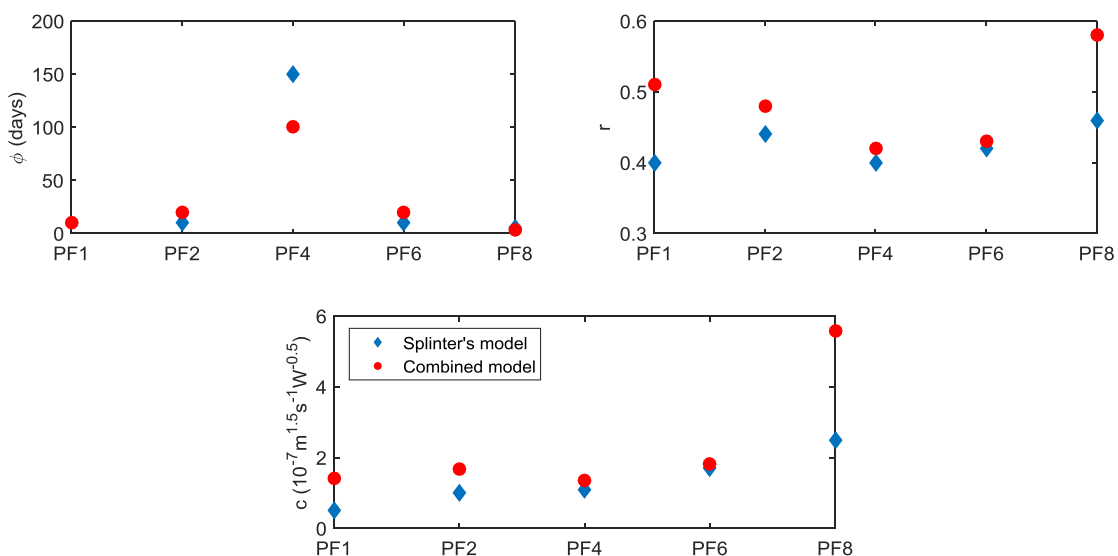


Figure 3: Comparison with results of Splinter *et al.* (2014). Top left panel: the 'memory decay' ϕ (days). Top right panel: the erosion ratio r . Bottom panel: the optimized free parameter c ($10^{-7} \text{m}^{1.5} \text{s}^{-1} \text{W}^{-0.5}$).

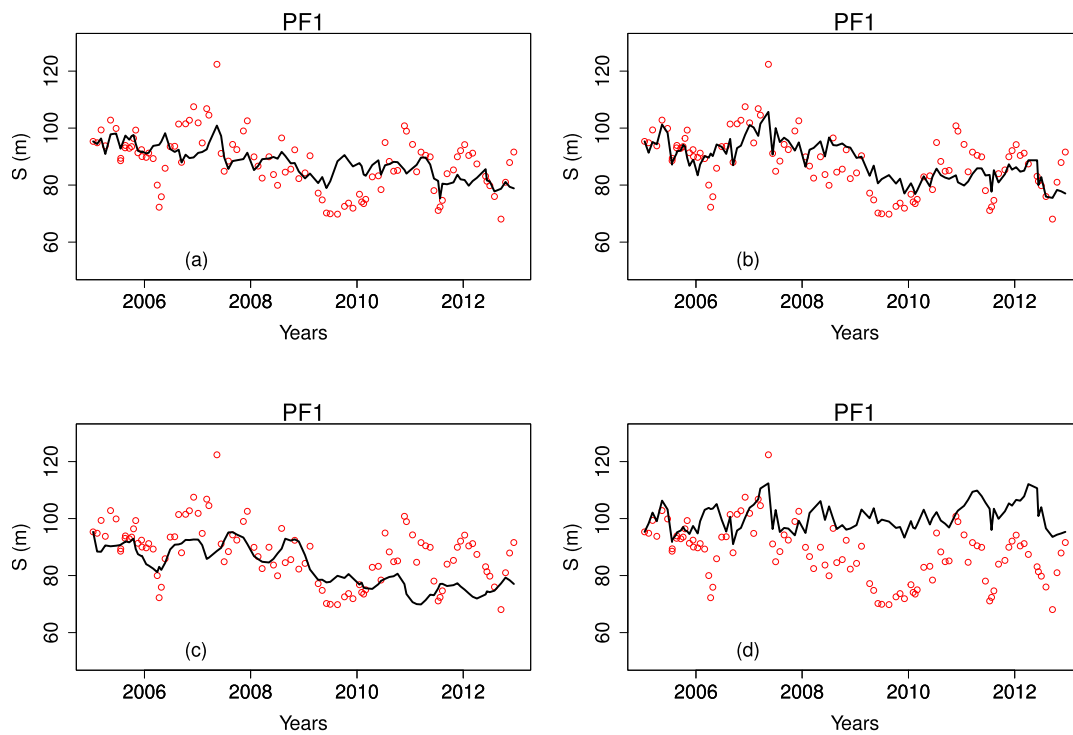


Figure 4: Time series of measured shoreline positions at PF1 (circles). Time series model shoreline positions at PF1 (solid line): (a) STDBCO14 cross-shore model. (b) combined model. (c) longshore contribution to the combined model. (d) cross-shore contribution to the combined model.

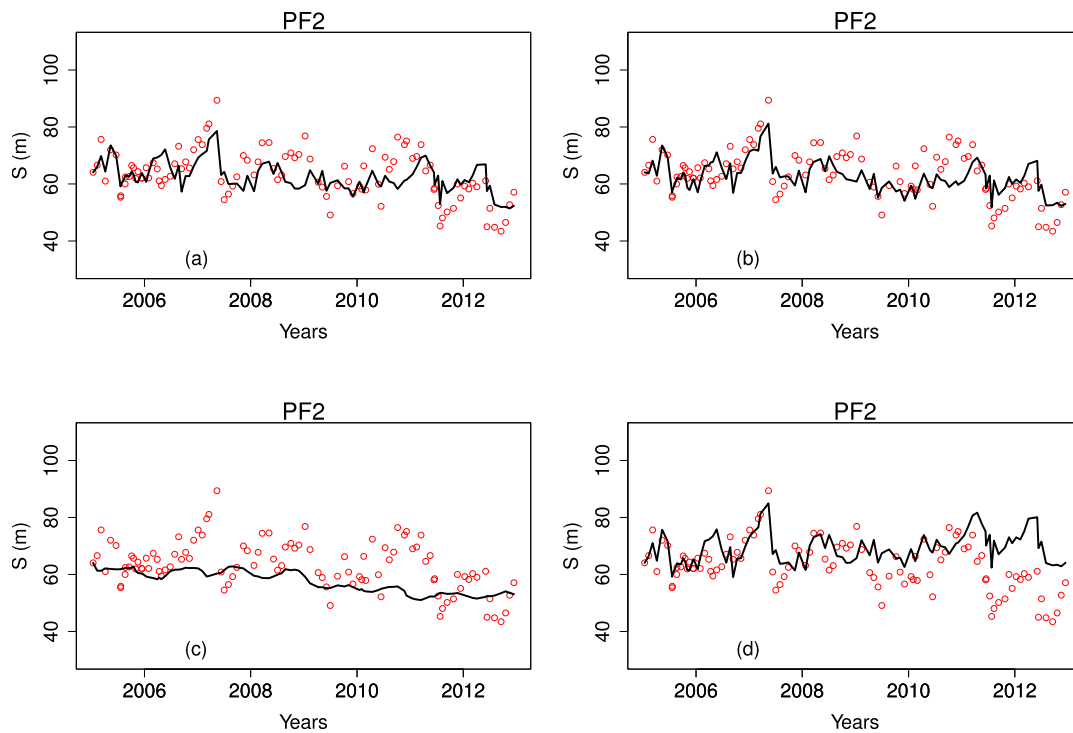


Figure 5: Time series of measured shoreline positions at PF2 (circles). Time series model shoreline positions at PF2 (solid line): (a) STDBCO14 cross-shore model. (b) combined model. (c) longshore contribution to the combined model. (d) cross-shore contribution to the combined model.

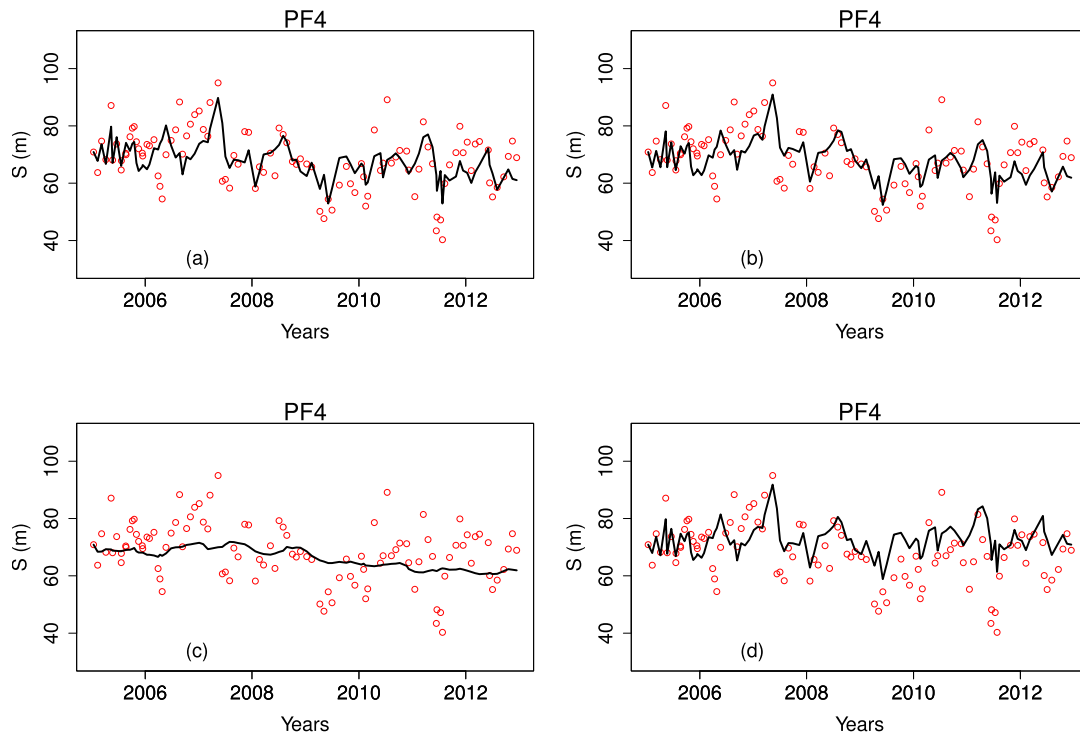


Figure 6: Time series of measured shoreline positions at PF4 (circles). Time series model shoreline positions at PF4 (solid line): (a) STDBCO14 cross-shore model. (b) combined model. (c) longshore contribution to the combined model. (d) cross-shore contribution to the combined model.

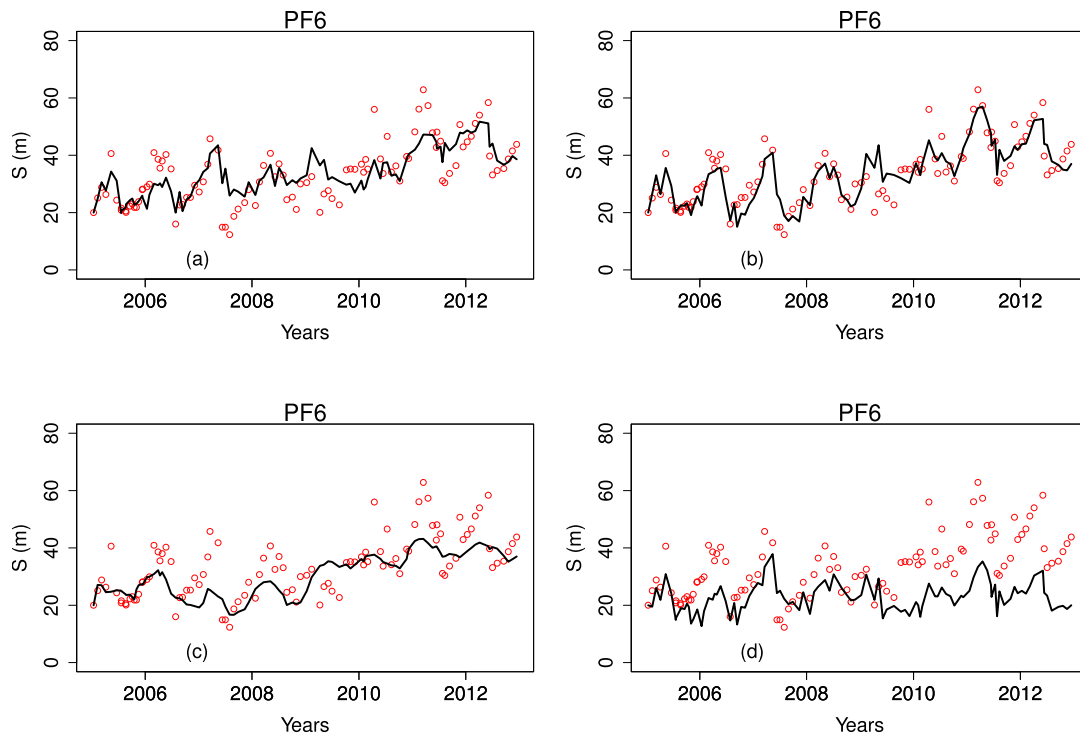


Figure 7: Time series of measured shoreline positions at PF6 (circles). Time series model shoreline positions at PF6 (solid line): (a) STDBCO14 cross-shore model. (b) combined model. (c) longshore contribution to the combined model. (d) cross-shore contribution to the combined model.

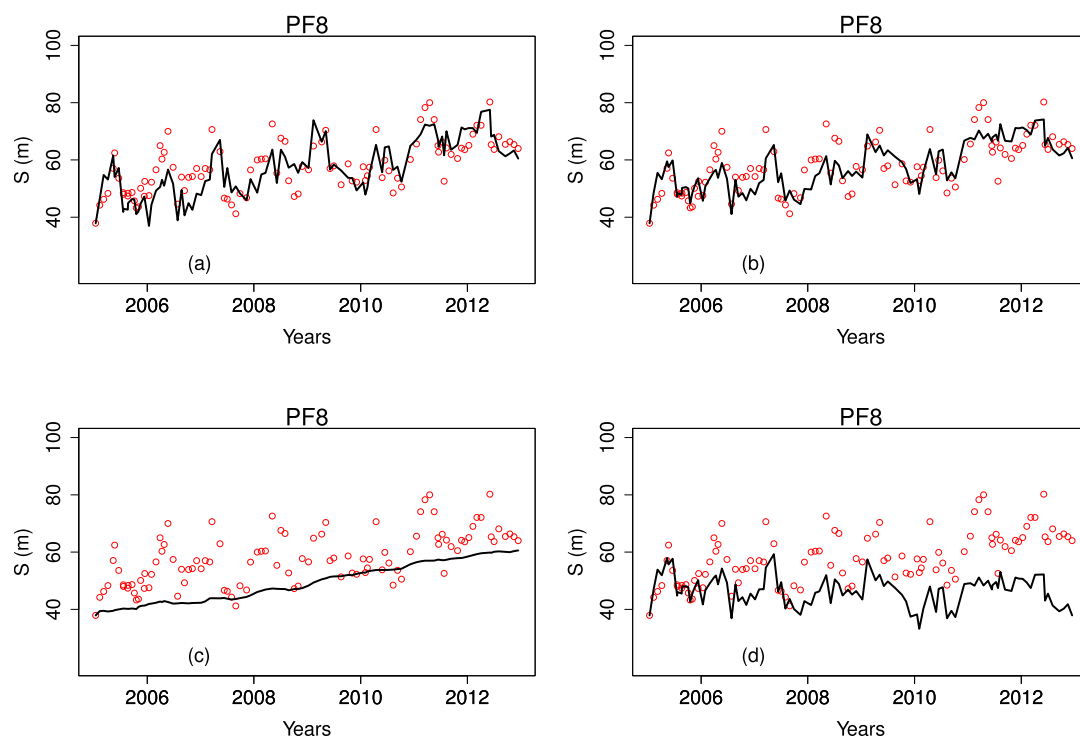


Figure 8: Time series of measured shoreline positions at PF8 (circles). Time series model shoreline positions at PF8 (solid line): (a) STDBC014 cross-shore model. (b) combined model. (c) longshore contribution to the combined model. (d) cross-shore contribution to the combined model.

Table 5: Free non-dimensional parameters a and b of the longshore model.

Transect	PF1	PF2	PF4	PF6	PF8
a	-0.0248	-0.0086	-0.004	0.007	0.0044
b	0.2176	0.1482	0.0947	-0.2999	-0.0674

5. Discussion and conclusion

Regarding the longshore contribution, it is undeniable that the longshore component provides the right trend of shoreline evolution on the calibration time range. This indicates that the d free parameter in equation (1) can be advantageously replaced by the longshore model. During this same time period, the beach is in an overall erosion tendency at PF1 and PF2 while at PF6 and PF8, the beach is accreting. The erosion at PF1 on the period is of the order of 20m. In addition, the longshore model gives a slight eroding trend at PF4 (approximately 10m) which indicates this transect is close to the pivotal point of the embayed beach. At PF1 and PF6, the longshore component not only gives the right long-term trend, but also contributes the seasonal shoreline changes. This finding indicates that part of the seasonal shoreline position fluctuations are also due to longshore transport. Moreover, it can be concluded that the longshore transport has a strong effect on PF1 and PF6 and that is why the longshore component contributes considerably more to the combined model at these two transects, and consequently provides smaller RMSEs in comparison with the other transects (Tab. 4). Despite having smaller RMSE, the shoreline calibration of the combined model is still not entirely satisfactory at PF1 (Fig. 3). It may be due to the location of PF1 close to a headland and in front of a shoal. This points at the need of a better estimation of the breaking wave characteristics by a method taking into account both the refraction and the diffraction of waves. While almost all transects have identical NMSEs with those of Splinter *et al.* (2014), PF6 has an obviously smaller NMSE (Tab. 4). It means PF6 is sensitive to the wave direction and longshore transport.

It should be stressed that a certain improvement of the skill of the model could be gained by offsetting the S computed values to minimize the RMSE, an option not taken here.

At all locations, the model produces variability in shoreline position which is far from that of the data which was also the case in Splinter *et al.* (2014). This cannot be improved by using the breaking significant wave height $H_{s,b}$ obtained from equation (28) since it has a smaller variability than that of $H_{s,10}$. Therefore, once again, $H_{s,10}$ was used for cross-shore component calibration instead of $H_{s,b}$.

It is noticeable that the equilibrium shoreline orientation for the longshore component as stated by equation (19) is expressed in terms of shoreline angle β and the breaking wave angle α_b . However, in this study, because the relation by equation (19) between β and α_b is unsatisfactory, we used the wave angle at $h = 10$ m for longshore component calibration. Here again we feel that improvements in breaking wave characteristics are required.

To conclude, the assumption of an equilibrium shoreline orientation related to longshore sediment transport was shown to be physically sound even though improvements in the breaking wave characteristics are required. The suggested longshore contribution to shoreline positions is completely able to describe the long-term trends of that position. Our new model which is a combination of a cross-shore model and longshore one gives an overall improvement, with smaller NMSE and RMSE, over a “pure” cross-shore model.

Acknowledgements

The first author is grateful to the Ambassade de France au Vietnam for granting her the Bourse d'Excellence. The work is funded by the MEPEIRA project of Grenoble INP, the CNRS MaGIL project and the University of Grenoble VIGIECOT project.

References

- Castelle, B., Marieu, V., Bujan, S., Ferreira, S., Parisot, J.-P., Capo, S., Senechal, N., & Chouzenoux, T., 2014. Equilibrium shoreline modelling of a high-energy meso-macrotidal multiple-barred beach. *Marine Geology*, 347: 85-94.
- Cheng, N.-S., 1997. Simplified settling velocity formula for sediment particle. *Journal of hydraulic engineering*, 123(2): 149-152.
- Davidson, M.A. & Turner, I.L., 2009. A behavioral template beach profile model for predicting seasonal to interannual shoreline evolution. *Journal of Geophysical Research: Earth Surface*, 114(F1).
- Davidson, M.A., Splinter, K.D. & Turner, I.L., 2013. A simple equilibrium model for predicting shoreline change. *Coastal Engineering*, 73: 191-202.
- Idier, D., Falqués, A., Ruessink, B.G., & Garnier, R., 2011. Shoreline instability under low-angle wave incidence. *Journal of Geophysical Research: Earth Surface*, 116(F4).
- Komar, P.D., 1974. *Beach processes and sedimentation*. Prentice-Hall, Englewood Cliffs, N.J.
- Kriebel, D.L., & Dean, R.G., 1993. Convolution method for time-dependent beach-profile response. *Journal of Waterway, Port, Coastal, and Ocean Engineering*, 119(2): 204-226.
- Pelnaud-Considère, R., 1956. Theoretical tests on the shoreline evolution of sand and gravel beaches.
- Reeve, D., Chadwick, A., & Fleming, C., 2004. *Coastal engineering: processes, theory and design practice*. CRC Press.
- Splinter, K.D., Turner, I.L., Davidson, M.A., Barnard, P., Castelle, B., & Oltman-Shay, J., 2014. A generalized equilibrium model for predicting daily to interannual shoreline response. *Journal of Geophysical Research: Earth Surface*, 119(9): 1936-1958
- Turki, I., Medina, R., Coco, G., & Gonzalez, M., 2013. An equilibrium model to predict shoreline rotation of pocket beaches. *Marine Geology*, 346: 220-232.
- Turner, I.L., Harley, M.D., Short, A.D., Simmons, J.A., Bracs, M.A., Phillips, M.S., & Splinter, K.D., 2016. A multi-decade dataset of monthly beach profile surveys and inshore wave forcing at Narrabeen, Australia. *Scientific data*, 3.
- Wright, L.D., & Short, A D., 1984. Morphodynamic variability of surf zones and beaches: a synthesis. *Marine Geology*, 56(1-4): 93-118.